Redshift Evolution of the Galaxy Velocity Dispersion Function

Bezanson, R.; Dokkum, P.G. van; Franx, M.; Brammer, G.B.; Brinchmann, J.; Kriek, M.; ... ; Williams, R.J.

The Astrophysical Journal Letters, 737:L31 (6pp), 2011 August 20 doi:10.1088/2041-8205/737/2/L31

REDSHIFT EVOLUTION OF THE GALAXY VELOCITY DISPERSION FUNCTION

Rachel Bezanson[1], Pieter G. van Dokkum[1], Marijn Franx[2], Gabriel B. Brammer[3], Jarle Brinchmann[2], Mariska Kriek[4], Ivo Labbé[2], Ryan F. Quadri[5,7], Hans-Walter Rix[6], Jesse van de Sande[2], Katherine E. Whitaker[1], and Rik J. Williams[5]
[1] Department of Astronomy, Yale University, New Haven, CT 06520-8101, USA
[2] Sterrewacht Leiden, Leiden University, NL-2300 RA Leiden, The Netherlands
[3] European Southern Observatory, Alonso de Crdova 3107, Casilla 19001, Vitacura, Santiago, Chile
[4] Harvard-Smithsonian Center for Astrophysics, Cambridge, MA, USA
[5] Carnegie Observatories, Pasadena, CA 91101, USA
[6] Max-Planck-Institut für Astronomie, Königstuhl 17, D-69117 Heidelberg, Germany
Received 2011 May 26; accepted 2011 July 5; published 2011 July 28

ABSTRACT

We present a study of the evolution of the galaxy velocity dispersion function (VDF) from $z = 0$ to $z = 1.5$ using photometric data from the Ultra-Deep and the NEWFIRM Medium-Band Survey in the COSMOS field. The VDF has been measured locally using direct kinematic measurements from the Sloan Digital Sky Survey (SDSS), but direct studies of the VDF at high redshift are difficult as they require velocity dispersion measurements of many thousands of galaxies. Taylor et al. demonstrated that dynamical and stellar masses are linearly related when the structure of the galaxy is accounted for. We show that the stellar mass, size, and Sérsic index can reliably predict the velocity dispersions of SDSS galaxies. We apply this relation to galaxies at high redshift and determine the evolution of the inferred VDF. We find that the VDF at $z \sim 0.5$ is very similar to the VDF at $z = 0$. At higher redshifts, we find that the number density of galaxies with dispersions $\lesssim$200 km s^{-1} is lower, but the number of high-dispersion galaxies is constant or even higher. At fixed cumulative number density, the velocity dispersions of galaxies with $\log N[\mathrm{Mpc}^{-3}] < -3.5$ increase with time by a factor of $\sim$1.4 from $z \sim 1.5$–0, whereas the dispersions of galaxies with lower number density are approximately constant or decrease with time. The VDF appears to show less evolution than the stellar mass function, particularly at the lowest number densities. We note that these results are still somewhat uncertain and we suggest several avenues for further calibrating the inferred velocity dispersions.

Key words: cosmology: observations – galaxies: elliptical and lenticular, cD – galaxies: evolution – galaxies: formation

Online-only material: color figures

1. INTRODUCTION

Stellar velocity dispersion is a fundamental property of galaxies. Through $M \propto R_\star \sigma_\star^2 / G$ it provides a characterization of the galaxy mass and is a key axis in the fundamental plane of early-type galaxies (e.g., Djorgovski & Davis 1987; Bernardi et al. 2003). Further, it appears to correlate strongly with many other properties of galaxies, such as specific star formation rates, galaxy color, and black hole mass (Magorrian et al. 1998; Franx et al. 2008; Trujillo et al. 2011).

The evolution of an individual galaxy's velocity dispersion carries information about the physical mechanisms responsible for its growth. Broadly, processes that increase mass more efficiently than size, such as central gas accretion and the resulting star formation, could increase velocity while processes such as minor merging or mass loss in galactic winds could increase the overall size of a galaxy and decrease the velocity dispersion. The central dispersions may also be fairly stable with time and reflect the central dark matter potentials at the time when the galaxy started forming (Loeb & Peebles 2003). In this scenario, high-redshift galaxies form the central regions of local massive galaxies and still retain signatures of their earliest progenitors.

Furthermore, central velocity dispersion lies at the intersection of observational properties and quantities predictable from simulations. Observational evidence about the shape and evolution of the VDF can be directly compared to predictions from cosmological simulations. Finally, masses of the supermassive black holes in the centers of galaxies display the strongest correlations with host galaxy velocity dispersions—understanding the distribution of velocity dispersions would hold further significance for the study of black holes and active galactic nuclei.

In the local universe, the velocity dispersion function (VDF) has been measured directly (e.g., Sheth et al. 2003; Mitchell et al. 2005; Choi et al. 2007). While measurements of stellar velocity dispersion are possible out to $z \sim 1$, they become prohibitive for large samples at $z > 1$. At $z = 0$ we can predict velocity dispersions of galaxies very well from their photometric properties. Here we present a new approach to describe the VDF based on photometric predictions and constrain its evolution out to $z \sim 1.5$. For this work we assume a concordance cosmology ($H_0 = 70$ km s^{-1} Mpc^{-1}, $\Omega_\mathrm{M} = 0.3$, and $\Omega_\Lambda = 0.7$).

2. DATA

2.1. Spectroscopic Redshifts, Velocity Dispersions, Sizes, and Stellar Masses at $z \sim 0$

The $z \sim 0$ data are based on the analysis of several publicly available catalogs from the Sloan Digital Sky Survey Data Release 7 (SDSS DR7). Galaxies are included from $0.05 < z < 0.07$, using photometric information from the main

[7] Hubble Fellow.

DR7 catalogs (Abazajian et al. 2009) and redshift and velocity dispersions from the Princeton pipeline. The sample is selected to have good photometric measurements with the SDSS Science Primary flag, and low relative errors in velocity dispersion (<10%). All velocity dispersions are aperture corrected to $r_e/8$ using $\sigma_0 = \sigma_{\rm ap}(8.0r_{\rm ap}/r_e)^{0.066}$ based on the best-fit correction to the SAURON sample (Cappellari et al. 2006), where $r_{\rm ap} = 1\farcs5$ is the radius of the SDSS spectroscopic fiber. We adopt the best-fit Sérsic (1968) effective radii in the r' band from the New York University Value-Added Galaxy Catalog (NYU-VAGC; Blanton et al. 2005). These sizes are based on fits to azimuthally averaged light profiles and are equivalent to circularized effective radii. Stellar masses are computed by the MPA-JHU group from the DR7 best-fit model magnitudes[8] (Brinchmann et al. 2004). We adopt these $M_\star/L$ ratios and derive stellar masses from the luminosity of the best-fit Sérsic model for all galaxies.

2.2. Sizes and Stellar Masses at $z > 0$

We use two samples of high-redshift galaxies in this Letter. The first is the 0.77 deg^2 UKIDSS Ultra-Deep Survey (UDS) K-selected galaxy catalog (Williams et al. 2009, 2010). This catalog includes near-infrared photometry (JHK) from the UKIDSS UDS (Lawrence et al. 2007; Warren et al. 2007), optical imaging from the Subaru/*XMM-Newton* Deep Survey (SXDS; Sekiguchi & SXDS 2004) and 3.6/4.5 μm data from the SWIRE survey (Lonsdale et al. 2003). Circularized effective radii ($r_e = \sqrt{ab}$) were measured in the J, H, and K images for all bright sources ($K < 22.4$) from Sérsic (1968) models fitted with GALFIT (Peng et al. 2002). A full description of the catalog and size fitting as well as associated tests can be found in Williams et al. (2010).

The second is the NEWFIRM Medium-Band Survey (NMBS) of the COSMOS field, which we briefly summarize below. For an in-depth description of the survey see Whitaker et al. (2011). The 0.21 deg^2 field includes medium-band NIR imaging ($J1$, $J2$, $J3$, $H1$, $H2$, K) from the Mayall 4 m telescope, optical imaging ($ugriz$) from the Canada–France–Hawaii Telescope Legacy Survey and Subaru, Infrared Array Camera imaging, and 24 μm data from the Multiband Imaging Photometer for *Spitzer* (MIPS). Sizes for the Cosmos galaxies are measured from the Ks WIRCam Deep Survey (WIRDS) $0\farcs186$ pixel^{-1} images (Bielby et al. 2011, in preparation), which have seeing of $\sim 0\farcs6$–$0\farcs7$ and the v.1.3 Advanced Camera for Surveys (ACS) F814W mosaic from Scoville et al. (2007). For details of galaxy modeling see P. G. van Dokkum et al. (2011, in preparation)—we summarize as follows. Circularized effective radii, axis ratio, and Sérsic indices are determined for all galaxies brighter than $K < 22$ using Sérsic models convolved with a position-dependent point-spread function (PSF) with GALFIT (Peng et al. 2002). We test our procedure using independent high spatial resolution data from a small area of overlapping Wide Field Camera 3 (WFC3) imaging from the 3D-HST survey (P. G. van Dokkum et al. 2011, in preparation). The interpolated WIRDS/ACS sizes are consistent with the WFC3 sizes down to $\sim 0\farcs15$ with a biweight mean of $\log(r_{e,\rm ACS\&WIRDS}/r_{e,\rm WFC3}) = 0\farcs0009$ and a scatter of 0.1 dex (Figure 1).

In both fields, sizes are measured down to an arbitrary limit; however, as most of these sizes are based on ground-based imaging we assign a minimum size for all galaxies of $r_e = 0\farcs2$.

[8] http://www.mpa-garching.mpg.de/SDSS/DR7/

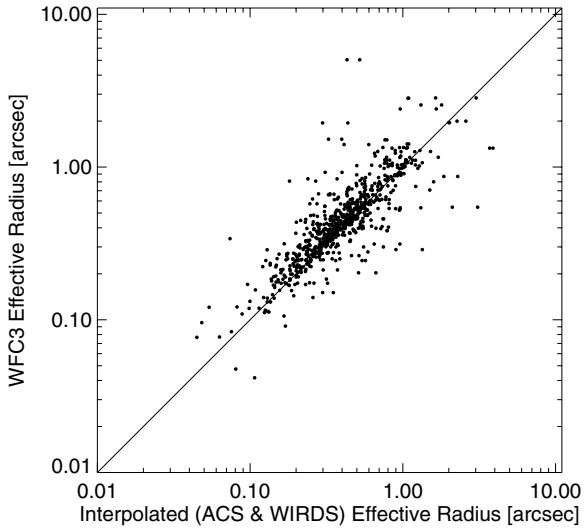

Figure 1. Sizes measured from WFC3 F140W imaging compared to sizes interpolated between measurements from ACS F814W and WIRDS Ks imaging.

Photometric redshifts for all galaxies in the UDS and COSMOS surveys were calculated using the EAZY code (Brammer et al. 2008). Stellar masses were computed using FAST (Kriek et al. 2009), from Bruzual & Charlot (2003) stellar population synthesis models with solar metallicity and a Chabrier (2003) initial mass function (IMF).

3. INFERRED VELOCITY DISPERSION

To derive a VDF at $z > 0$, we now describe how to estimate the stellar velocity dispersion of galaxies from their photometric properties. According to the virial theorem, the dynamical mass of a galaxy is proportional to the product of the square of its measured dispersion and effective radius:

$$M_{\rm dyn} = K_v \sigma_0^2 r_e / G. \quad (1)$$

Stellar mass has been shown to be proportional to dynamical mass for local galaxies (e.g., Taylor et al. 2010). However, Taylor et al. (2010) demonstrated that simple estimates of dynamical mass based on homology exhibit residual trends with galaxy structural properties and introduced a more robust structure-corrected dynamical mass, which we use to calculate inferred velocity dispersion based on photometric estimates of stellar mass and observed size. We adopt a Sérsic-dependent virial constant, $K_v(n)$ (Bertin et al. 2002):

$$K_v(n) = \frac{73.32}{10.465 + (n - 0.94)^2} + 0.954. \quad (2)$$

In order to predict the central velocity dispersion of a galaxy based on its size and stellar mass, we define

$$\sigma_{\rm inf} = \sqrt{\frac{GM_{\rm dyn}}{K_v(n) r_e}} = \sqrt{\frac{GM_\star}{K_\star(n) r_e}}, \quad (3)$$

where $K_\star(n) \equiv K_v(n)(\frac{M_\star}{M_{\rm dyn}})$. Since Taylor et al. (2010) showed that $K_v(n)(\frac{M_\star}{M_{\rm dyn}})$ depends only weakly on mass, we adopt the average ratio of stellar to total mass, calibrated such that the median $\sigma_{\rm inf} = \sigma_0$ for $2.0 < \log\sigma_0 < 2.4$ in the SDSS. We find that $\langle \frac{M_\star}{M_{\rm dyn}} \rangle = 0.557$, therefore $K_\star(n) = 0.557 K_v(n)$. The central

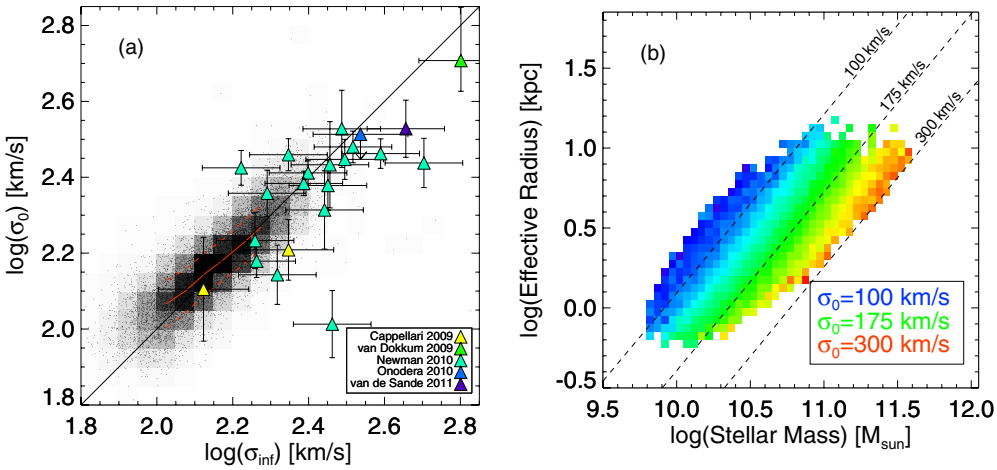

Figure 2. (a) Measured central velocity dispersion vs. inferred velocity dispersion of galaxies in the SDSS DR7. Galaxies are binned by $\log \sigma_{\rm inf} = 0.05$ and the running mean and rms are shown in red for bins containing at least 100 galaxies. There is a very good correlation with a scatter of ∼0.06 dex. High-redshift ($1 < z < 2.5$) galaxies are included as large colored triangles. (b) Effective radii from NYU-VAGC best-fit Sérsic models in the r' band vs. stellar mass in the SDSS, color-coded by median measured velocity dispersion. Lines of constant inferred dispersion are included as dashed black lines. Both panels illustrate that the stellar mass and size of galaxies can be used to predict velocity dispersions.

(A color version of this figure is available in the online journal.)

and inferred velocity dispersions agree well for the SDSS, with a 1σ error of 0.06 dex (Figure 2(a)). This is remarkable, particularly when considering that no morphological selections are applied: after applying the Sérsic-dependent virial constant, this relation holds for both ellipticals and spiral galaxies. This implies that the velocity dispersion, σ_0, can be well predicted from $M_\star$ and r_e. Figure 2(b) shows the size–mass relation for SDSS, colored by median measured dispersion for bins including a minimum of five galaxies. We use the median $n(M_\star)$ to overplot lines of constant inferred dispersion. Again, the measured and inferred dispersions agree quite well.

Also included in Figure 2(a) are published measurements for galaxies at $1.0 < z < 2.5$ (Cappellari et al. 2009; van Dokkum et al. 2009; Newman et al. 2010; Onodera et al. 2010; van de Sande et al. 2011; large colored triangles), assuming errors due to spectral energy distribution modeling of $M_\star = 0.2$ dex. The biweight mean offset in $\sigma_0/\sigma_{\rm inf}$ is small (-0.056 ± 0.025 dex) and the high observed scatter of 0.131 ± 0.028 dex is fully consistent with scatter due to measurement errors. The relation does not appear to evolve significantly out to high redshift, but we emphasize that current samples of high-z dynamical measurements are small and biased toward high dispersions. Motivated by Figure 2(a) we assume that the SDSS relations between velocity dispersion, stellar mass, effective radius, and Sérsic index do not evolve with redshift and calculate inferred dispersions for the UDS and COSMOS catalogs. To limit bandpass-dependent effects, we calculate $\sigma_{\rm inf}$ separately using UKIDSS J and K sizes for the UDS and ACS F814W and WIRDS Ks sizes for COSMOS. Next, we interpolate $\sigma_{\rm inf}$ to a rest-frame wavelength of 6200 Å, the central wavelength of the r' filter. We note that for apparently extremely compact galaxies with measured sizes $<0\farcs2$, these can be interpreted as minimum inferred velocity dispersions.

4. VELOCITY DISPERSION FUNCTION

A number of estimates of the $z \sim 0$ VDF of early-type galaxies exist based on the SDSS (Sheth et al. 2003; Mitchell et al. 2005; Choi et al. 2007; Chae 2010). These studies are in reasonably good agreement and show that the $z = 0$ VDF appears to be well fit by modified Schechter (1976) functions. Sheth et al. (2003) present a correction to the VDF for the contribution due to late-type galaxies, based on circular velocities. In the top row of Figure 3 we show both the fit to the early-type VDF (thin dotted black lines) and the total VDF (thick solid black lines), which includes the correction for late-type galaxies. This latter function is calculated by fitting a polynomial to the data in Figure 6 in Sheth et al. (2003).

Measurement errors of velocity dispersions have a non-negligible effect on the shape of the inferred VDF, particularly on the steep, high dispersion tail. We model this effect by producing a mock catalog that intrinsically follows the total Sheth et al. (2003) VDF. In Section 3, we measured a scatter of 0.06 dex in inferred dispersion, which is comprised of intrinsic scatter in this relation combined with measurement errors in velocity dispersion. From the median relative error in velocity dispersion for galaxies with $\sigma \geqslant 200\,{\rm km\,s^{-1}}$ (0.028 dex), we estimate that the intrinsic scatter in the relation between measured and inferred dispersion is 0.053 dex. The thick dashed black lines in Figure 3 show the SDSS VDF when this scatter is added to the mock velocity dispersions.

The top panel of Figure 3 shows the inferred VDF for each field in all redshift ranges and values are included in Table 1. Errors reflect Poisson errors in each velocity dispersion bin. Incompleteness is mostly caused by galaxies that are too faint to measure reliable sizes. We define the dispersion completeness limit (gray regions in Figure 3) for each field and redshift range as the dispersion at which the 95% completeness plus 0.06 dex scatter about a linear fit to the K magnitude-inferred dispersion relation reaches the magnitude limit of the size catalogs.

In the lowest redshift range, $0.3 < z < 0.6$, the observed VDF matches the local VDF quite well in the region dominated by early-type galaxies, especially when compared to the scattered VDF. At low dispersions the $z \sim 0.5$ function is intermediate between the $z = 0$ VDF for early-types only (black dashed line) and for all galaxies (black solid line). In the higher redshift bins, the VDF appears to flatten. Low-dispersion galaxies become less common and high-dispersion galaxies more common, with an approximately constant crossover point. The colored points

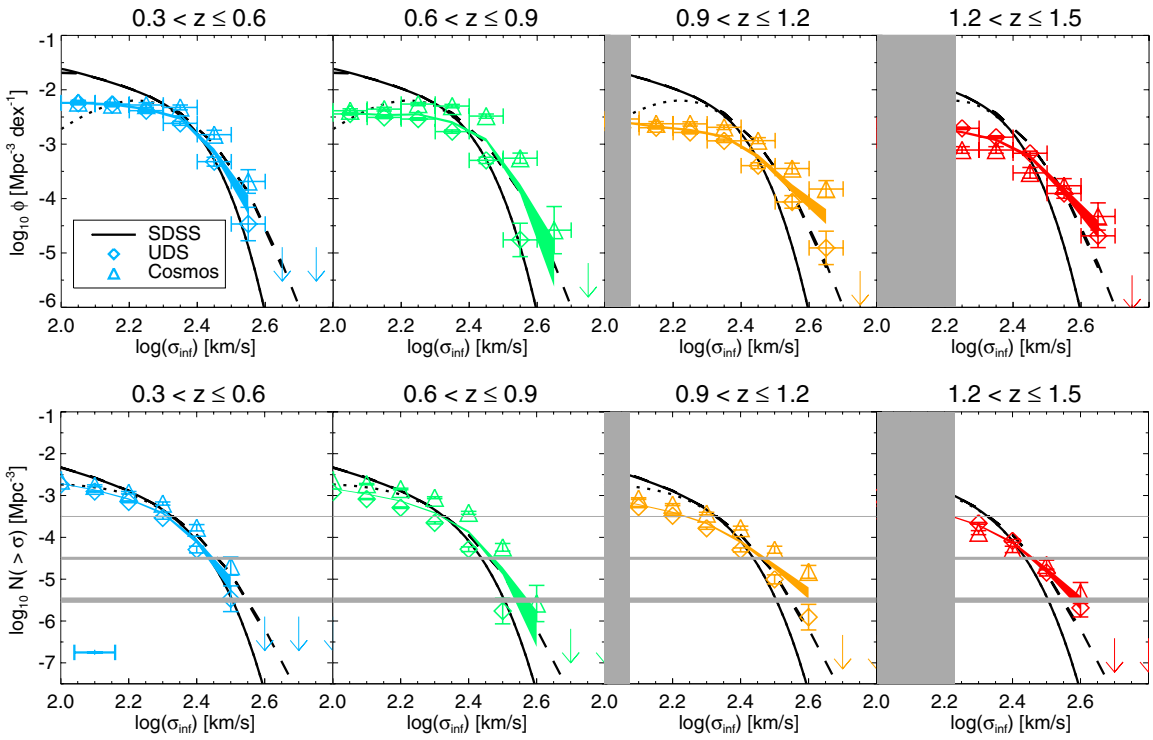

Figure 3. Top row: VDFs locally (black) as measured from SDSS and at higher redshifts for the two fields (color). Best-fit modified Schechter (1976) fits to the SDSS measured VDF are shown from Sheth et al. (2003) (thin dotted: early-type VDF; thick solid: total VDF; thick dashed: total scattered VDF). Higher redshift number densities are based on inferred velocity dispersions assuming $z = 0$ calibration. Individual colored lines reflect the measured VDF in each field (solid for UDS and dashed for COSMOS) and the circular data points show the volume-weighted average. Bottom row: cumulative VDFs for each redshift bin. Colors and symbols are the same as above. Three cuts in number density (horizontal gray lines) highlight three possible evolutionary behaviors. Galaxies at the lowest number density threshold, $\log N[\mathrm{Mpc}^{-3}] < -5.5$, increase in velocity dispersion from a redshift $z \sim 1.5$ to $z \sim 0$. Galaxies at a number density of $\log N[\mathrm{Mpc}^{-3}] < -4.5$ appear to be near the crossover and experience little evolution in velocity dispersion to $z \sim 0$. Finally, galaxies at the highest number density threshold of $\log N[\mathrm{Mpc}^{-3}] < -3.5$ appear to decrease in velocity dispersion with time.

(A color version of this figure is available in the online journal.)

show results for the UDS (diamonds) and COSMOS (triangles) fields separately. The flattening of the VDF with redshift is seen in both fields, suggesting that it is not due to field-to-field variations. We note that the COSMOS field has a cluster at $z = 0.7$ and an overdensity at $z \sim 1.0$ (Whitaker et al. 2011). These structures are reflected in the higher normalization of the COSMOS VDF in the second and third redshift bins.

5. CUMULATIVE VELOCITY DISPERSION FUNCTION

We also consider the evolution of velocity dispersions of galaxies at constant cumulative number density. Assuming that the rank order of galaxies remains the same, a number density selection selects the same population of galaxies as a function of redshift (e.g., Wake et al. 2008; van Dokkum et al. 2010). We show the cumulative VDF in the bottom row of Figure 3 and select galaxies at three number densities: $\log N[\mathrm{Mpc}^{-3}] = -3.5, -4.5$, and -5.5 (horizontal gray lines). The crossing point between each number density threshold and the cumulative VDF evolves differently with redshift.

In Figure 4, we show the evolution of the velocity dispersion at fixed cumulative number density (σ_{cross}) with redshift. The rare high-dispersion galaxies ($\log N[\mathrm{Mpc}^{-3}] < -5.5$) exhibit a weak trend with even higher dispersions at high redshift and a slope of 0.066 ± 0.059. While it is difficult to decrease galaxy's velocity dispersion with time, it has been suggested that this can occur via extensive minor merging, which can efficiently increase size while slowly increasing mass (e.g., Bezanson et al. 2009; Hopkins et al. 2009; van Dokkum et al. 2010). An abundance of evidence has demonstrated that at a given mass, galaxies have smaller sizes at high redshift than in the local universe (e.g., Daddi et al. 2005; Trujillo et al. 2006; van Dokkum et al. 2008; Cimatti et al. 2008; van der Wel et al. 2008; Franx et al. 2008; Damjanov et al. 2009). We emphasize that these are the most extreme galaxies in the universe—with inferred velocity dispersions of $\gtrsim 400\,\mathrm{km\,s^{-1}}$ at $z \sim 0$. The fact that this trend is weak suggests that the structure correction to the inferred dispersions may mitigate the evolution in density within r_e. At the higher threshold of $\log N[\mathrm{Mpc}^{-3}] < -4.5$ galaxies appear to have already attained the central velocity dispersions that they will have at $z = 0$, with a slope of 0.014 ± 0.054. If these galaxies maintain constant central dispersion while continuing to evolve from $z \sim 1.5$ to the present it could be evidence that they are undergoing inside-out growth in which the central dynamics of the stars are set by some early processes and the overall structure of the galaxy builds up around the core or that they undergo size growth at the same rate as mass growth. Finally, for the galaxies above the highest density threshold of $\log N[\mathrm{Mpc}^{-3}] < -3.5$ velocity dispersion increases with time. In this case the negative slope of -0.098 ± 0.053 is significant. This may suggest the importance of gas accretion and star formation, which could increase the stellar masses of the galaxies.

We note that the dispersion function appears to evolve slower than the stellar mass function: stellar mass increases by a factor of ~ 2 for the most extreme galaxies ($\log M_\star > 11$)

Table 1
Inferred and Cumulative Velocity Dispersion Functions

$\log \sigma_{\rm inf}$ (km s^{-1})		2.0–2.1	2.1–2.2	2.2–2.3	2.3–2.4	2.4–2.5	2.5–2.6	2.6–2.7
Redshifts	Field	$\log \Phi$[Mpc^{-3} dex^{-1}]						
$0.3 < z \leqslant 0.6$	UDS	-2.25 ± 0.02	-2.27 ± 0.02	-2.38 ± 0.03	-2.62 ± 0.04	-3.32 ± 0.08	-4.47 ± 0.31	< -4.77
	COSMOS	-2.24 ± 0.04	-2.27 ± 0.04	-2.28 ± 0.04	-2.32 ± 0.05	-2.83 ± 0.08	-3.69 ± 0.22	< -4.29
	Total	-2.24 ± 0.02	-2.27 ± 0.02	-2.36 ± 0.02	-2.52 ± 0.03	-3.14 ± 0.06	-4.11 ± 0.18	< -4.89
$0.6 < z \leqslant 0.9$	UDS	-2.44 ± 0.02	-2.51 ± 0.02	-2.54 ± 0.02	-2.77 ± 0.03	-3.30 ± 0.06	-4.76 ± 0.31	< -5.06
	COSMOS	-2.38 ± 0.03	-2.36 ± 0.03	-2.26 ± 0.03	-2.30 ± 0.03	-2.48 ± 0.04	-3.26 ± 0.09	-4.58 ± 0.43
	Total	-2.43 ± 0.02	-2.46 ± 0.02	-2.45 ± 0.02	-2.60 ± 0.02	-2.92 ± 0.03	-3.82 ± 0.09	-5.19 ± 0.43
$0.9 < z \leqslant 1.2$	UDS	-2.62 ± 0.02	-2.70 ± 0.02	-2.78 ± 0.03	-2.94 ± 0.03	-3.40 ± 0.05	-4.06 ± 0.12	-4.91 ± 0.31
	COSMOS	-2.54 ± 0.03	-2.62 ± 0.04	-2.63 ± 0.04	-2.69 ± 0.04	-2.93 ± 0.06	-3.45 ± 0.10	-3.82 ± 0.15
	Total	-2.60 ± 0.02	-2.68 ± 0.02	-2.74 ± 0.02	-2.86 ± 0.03	-3.23 ± 0.04	-3.81 ± 0.08	-4.33 ± 0.14
$1.2 < z \leqslant 1.5$	UDS	-2.65 ± 0.02	-2.64 ± 0.02	-2.71 ± 0.02	-2.87 ± 0.03	-3.17 ± 0.04	-3.91 ± 0.09	-4.68 ± 0.22
	COSMOS	-2.94 ± 0.05	-2.92 ± 0.05	-3.11 ± 0.06	-3.11 ± 0.06	-3.53 ± 0.10	-3.76 ± 0.13	-4.33 ± 0.25
	Total	-2.70 ± 0.02	-2.69 ± 0.02	-2.78 ± 0.02	-2.92 ± 0.02	-3.23 ± 0.04	-3.87 ± 0.07	-4.57 ± 0.16
$\log \sigma_{\rm inf}$ (km s^{-1})		>2.0	>2.1	>2.2	>2.3	>2.4	>2.5	>2.6
Redshifts	Field	$\log N$[Mpc^{-3}]						
$0.3 < z \leqslant 0.6$	UDS	-1.74 ± 0.01	-1.90 ± 0.02	-2.15 ± 0.02	-2.53 ± 0.03	-3.29 ± 0.08	-4.47 ± 0.31	< -4.77
	COSMOS	-1.64 ± 0.02	-1.77 ± 0.02	-1.93 ± 0.03	-2.19 ± 0.04	-2.77 ± 0.08	-3.69 ± 0.22	< -4.29
	Total	-1.71 ± 0.01	-1.87 ± 0.01	-2.09 ± 0.02	-2.42 ± 0.03	-3.09 ± 0.05	-4.11 ± 0.18	< -4.89
$0.6 < z \leqslant 0.9$	UDS	-1.93 ± 0.01	-2.08 ± 0.01	-2.29 ± 0.02	-2.65 ± 0.03	-3.28 ± 0.06	-4.76 ± 0.31	< -5.06
	COSMOS	-1.64 ± 0.01	-1.73 ± 0.02	-1.84 ± 0.02	-2.05 ± 0.02	-2.41 ± 0.04	-3.24 ± 0.09	-4.58 ± 0.43
	Total	-1.84 ± 0.01	-1.96 ± 0.01	-2.13 ± 0.01	-2.41 ± 0.02	-2.87 ± 0.03	-3.81 ± 0.09	-5.19 ± 0.43
$0.9 < z \leqslant 1.2$	UDS	-2.11 ± 0.01	-2.28 ± 0.01	-2.48 ± 0.02	-2.78 ± 0.03	-3.30 ± 0.05	-4.00 ± 0.11	-4.91 ± 0.31
	COSMOS	-1.94 ± 0.02	-2.07 ± 0.02	-2.22 ± 0.02	-2.43 ± 0.03	-2.78 ± 0.05	-3.30 ± 0.08	-3.82 ± 0.15
	Total	-2.06 ± 0.01	-2.22 ± 0.01	-2.40 ± 0.01	-2.66 ± 0.02	-3.10 ± 0.03	-3.70 ± 0.07	-4.33 ± 0.14
$1.2 < z \leqslant 1.5$	UDS	-2.06 ± 0.01	-2.19 ± 0.01	-2.38 ± 0.02	-2.66 ± 0.02	-3.08 ± 0.03	-3.84 ± 0.08	-4.68 ± 0.22
	COSMOS	-2.35 ± 0.03	-2.48 ± 0.03	-2.68 ± 0.04	-2.89 ± 0.05	-3.29 ± 0.08	-3.66 ± 0.12	-4.33 ± 0.25
	Total	-2.12 ± 0.01	-2.25 ± 0.01	-2.44 ± 0.01	-2.71 ± 0.02	-3.13 ± 0.03	-3.79 ± 0.07	-4.57 ± 0.16

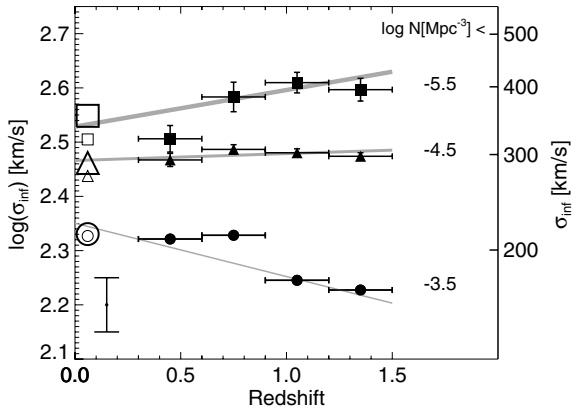

Figure 4. Velocity dispersion at the three number density thresholds ($\log N$[Mpc^{-3}] $= -3.5, -4.5,$ and -5.5) shown in the bottom row of Figure 3. Open symbols represent the unscattered (small symbols) and scattered (large symbols; Sheth et al. 2003) total VDF. Filled symbols represent $\sigma_{\rm cross}$ for the higher redshift VDFs. Vertical error bars include the 0.06 dex error in inferred velocity dispersion divided by the square root of the number of galaxies interpolated between two nearest bins in $\log \sigma$ from Figure 3. We include an additional error of 0.05 dex (error bar in the lower left corner), added in quadrature to all points, to encompass additional sources of error.

from $z \sim 2$–0, with even stronger evolution at lower masses (Brammer et al. 2011).

6. DISCUSSION

We stress that all of these results are preliminary and rest on a multitude of assumptions. First of all, our samples of galaxies with size measurements may suffer from incompleteness, especially at the low mass limit. We have tried to place thresholds above which our sample should be complete, however these limits may be underestimated.

The majority of galaxy sizes are measured from ground-based imaging, which could be uncertain, especially for compact galaxies at high redshift. In Figure 1, we have shown that the WIRDS/ACS sizes agree quite well with those measured from WFC3, exhibiting a scatter of only 0.1 dex. However, at the high dispersion end of the VDF, the accuracy of individual size measurements becomes more important than overall trends. Future studies would benefit from careful fitting of profiles exclusively based on space-based imaging. This will also improve the accuracy of our Sérsic indices.

The most tentative assumption remains that the relation between inferred and measured velocity dispersions does not evolve. There are many factors that contribute to this relation. Aperture corrections depend on galaxy profiles and therefore any systematic evolution in the light distribution of galaxies would affect the measured velocity dispersions. However, this is a relatively weak effect as the aperture corrections are small. More important may be the dependence of K_v on Sérsic index, which could evolve if galaxy structure evolves in complex ways. Furthermore, our calibration of $K_\star(n)$ depends strongly on the average ratio of stellar to total dynamical mass, which may evolve with time and depend on the stellar mass of the galaxy. Taylor et al. (2010) found that $M_\star/M_{{\rm dyn},n}$ still exhibits trends with stellar mass at fixed n, suggesting that even at $z = 0$ the models for $K_v(n)$ do not completely describe the non-homology of galaxies. Any of these effects could preferentially influence certain types of galaxies, introducing systematic trends in the shape of the σ_0 versus $\sigma_{\rm inf}$ relation. The scatter in the relation

may also evolve with time; this could explain the apparent increase in the number of galaxies with high inferred dispersions at $z \gtrsim 0.6$. Finally, we assume a constant Chabrier (2003) IMF, which could also differ with redshift or halo mass (e.g., van Dokkum & Conroy 2010).

Measuring the entire VDF using dynamical measurements would require an extremely large spectroscopic survey. A more economical approach is to better calibrate the evolution of the inferred VDF. With a large sample of uniformly selected galaxies spanning a large range of velocity dispersions and lower measurement errors, one could characterize $\sigma_{\rm inf}$ as a function of stellar mass, Sérsic fits, and redshift.

Finally, we note that Chae (2010) measured the VDF in a similar redshift range ($z \sim 0.3$–1.0) from 30 lensing galaxies and found quite different results. Chae finds that at the low dispersion end ($\log\sigma \lesssim 2.3$) the VDF of galaxies agrees quite well with the local VDF, and that it steepens at higher redshift. At the high dispersion end, the Chae (2010) results are based on a lack of arcs with large separations. It is possible that this sample of lensing galaxies preferentially misses such lenses. Alternatively, it is possible that the intrinsic VDF does fall below the local VDF at high dispersions, but the scatter increases rapidly with redshift, producing the opposite evolution in our study. Further calibration of the inferred velocity dispersions at higher redshift is necessary to probe whether the two results are inconsistent.

Although measurements of the VDF at higher redshift may never be as precise as those measured from the SDSS, study of the evolution of the inferred VDF using more accurate and redshift-dependent dynamical calibrations will be a powerful tool for studying the growth and evolution of galaxies and the halos that they occupy.

We thank the referee for his/her feedback and acknowledge support from NSF grant AST-0807974 and *HST* grant GO-12177.01A.

REFERENCES

Abazajian, K. N., Adelman-McCarthy, J. K., Agüeros, M. A., et al. 2009, ApJS, 182, 543
Bernardi, M., Sheth, R. K., Annis, J., et al. 2003, AJ, 125, 1866
Bertin, G., Ciotti, L., & Del Principe, M. 2002, A&A, 386, 149
Bezanson, R., van Dokkum, P. G., Tal, T., et al. 2009, ApJ, 697, 1290
Blanton, M. R., Schlegel, D. J., Strauss, M. A., et al. 2005, AJ, 129, 2562
Brammer, G. B., van Dokkum, P. G., & Coppi, P. 2008, ApJ, 686, 1503
Brammer, G. B., Whitaker, K. E., van Dokkum, P. G., et al. 2011, arXiv:1104.2595
Brinchmann, J., Charlot, S., White, S. D. M., et al. 2004, MNRAS, 351, 1151
Bruzual, G., & Charlot, S. 2003, MNRAS, 344, 1000
Cappellari, M., Bacon, R., Bureau, M., et al. 2006, MNRAS, 366, 1126
Cappellari, M., di Serego Alighieri, S., Cimatti, A., et al. 2009, ApJ, 704, L34
Chabrier, G. 2003, PASP, 115, 763
Chae, K. 2010, MNRAS, 402, 2031
Choi, Y., Park, C., & Vogeley, M. S. 2007, ApJ, 658, 884
Cimatti, A., Cassata, P., Pozzetti, L., et al. 2008, A&A, 482, 21
Daddi, E., Renzini, A., Pirzkal, N., et al. 2005, ApJ, 626, 680
Damjanov, I., McCarthy, P. J., Abraham, R. G., et al. 2009, ApJ, 695, 101
Djorgovski, S., & Davis, M. 1987, ApJ, 313, 59
Franx, M., van Dokkum, P. G., Schreiber, N. M. F., et al. 2008, ApJ, 688, 770
Hopkins, P. F., Bundy, K., Murray, N., et al. 2009, MNRAS, 398, 898
Kriek, M., van Dokkum, P. G., Labbé, I., et al. 2009, ApJ, 700, 221
Lawrence, A., Warren, S. J., Almaini, O., et al. 2007, MNRAS, 379, 1599
Loeb, A., & Peebles, P. J. E. 2003, ApJ, 589, 29
Lonsdale, C. J., Smith, H. E., Rowan-Robinson, M., et al. 2003, PASP, 115, 897
Magorrian, J., Tremaine, S., Richstone, D., et al. 1998, AJ, 115, 2285
Mitchell, J. L., Keeton, C. R., Frieman, J. A., & Sheth, R. K. 2005, ApJ, 622, 81
Naab, T., Johansson, P. H., & Ostriker, J. P. 2009, ApJ, 699, L178
Newman, A. B., Ellis, R. S., Treu, T., & Bundy, K. 2010, ApJ, 717, L103
Onodera, M., Daddi, E., Gobat, R., et al. 2010, ApJ, 715, L6
Peng, C. Y., Ho, L. C., Impey, C. D., & Rix, H.-W. 2002, AJ, 124, 266
Schechter, P. 1976, ApJ, 203, 297
Scoville, N., Aussel, H., Brusa, M., et al. 2007, ApJS, 172, 1
Sekiguchi, K. SXDS. 2004, BAAS, 36, 1478
Sérsic, J. L. 1968, Atlas de Galaxias Australes (Cordoba: Observatorio Astronomico)
Sheth, R. K., Bernardi, M., Schechter, P. L., et al. 2003, ApJ, 594, 225
Taylor, E. N., Franx, M., Brinchmann, J., van der Wel, A., & van Dokkum, P. G. 2010, ApJ, 722, 1
Trujillo, I., Ferreras, I., & de la Rosa, I. G. 2011, arXiv:1102.3398
Trujillo, I., Förster, S., Natascha, M., et al. 2006, ApJ, 650, 18
van der Wel, A., Holden, B. P., Zirm, A. W., et al. 2008, ApJ, 688, 48
van de Sande, J., Kriek, M., Franx, M., et al. 2011, ApJ, 736, L9
van Dokkum, P. G., & Conroy, C. 2010, Nature, 468, 940
van Dokkum, P. G., Franx, M., Kriek, M., et al. 2008, ApJ, 677, L5
van Dokkum, P. G., Kriek, M., & Franx, M. 2009, Nature, 460, 717
van Dokkum, P. G., Whitaker, K. E., Brammer, G., et al. 2010, ApJ, 709, 1018
Wake, D. A., Sheth, R. K., Nichol, R. C., et al. 2008, MNRAS, 387, 1045
Warren, S. J., Hambly, N. C., Dye, S., et al. 2007, MNRAS, 375, 213
Whitaker, K. E., Labbé, I., van Dokkum, P. G., et al. 2011, ApJ, 735, 86
Williams, R. J., Quadri, R. F., Franx, M., van Dokkum, P., & Labbé, I. 2009, ApJ, 691, 1879
Williams, R. J., Quadri, R. F., Franx, M., et al. 2010, ApJ, 713, 738